

# Comparison Between Ultrasonic Vibration-Assisted Upsetting and Conventional Upsetting

YANXIONG LIU, SERGEY SUSLOV, QINGYOU HAN, LIN HUA, and CLAUSE XU

Ultrasonic vibration has been increasingly applied to metal forming processes due to its beneficial effects on the reduction of the forming force, flow stress, and friction coefficient and on the increase of the forming limit of the sheet metal. In this work, the effect of the ultrasonic vibration on the upsetting has been studied experimentally and numerically. The microstructure of the specimens processed with ultrasonic vibration-assisted upsetting (UAU) and conventional upsetting was characterized. Differences in the forming characteristics between these two methods, in terms of metal flow and forming force, were analyzed. The results of this study indicate that the use of high-intensity ultrasonic vibration can induce severe plastic deformation and improve the grain refinement efficiency. The grains of the specimens processed by the UAU process were refined to 100 to 300 nm. A deformation mechanism of the UAU process was proposed. The grain refinement mechanism was used to explain the reason why ultrasonic vibration can be used to improve the grain refinement efficiency of the upsetting process.

DOI: 10.1007/s11661-013-1651-9

© The Minerals, Metals & Materials Society and ASM International 2013

## I. INTRODUCTION

ULTRASONIC vibration has been widely applied to metal forming processes since the 1960s. The advantages of the application of the ultrasonic vibration in materials processing can be divided into two aspects: enhancing the forming processes and improving the microstructure and hence the mechanical properties of the specimen which was processed.

For the first aspect, the superposition of ultrasonic vibration on the metal forming process is capable of reducing the forming force and the friction coefficient and increasing the forming limit. For example, Daud *et al.*<sup>[1]</sup> superimposed ultrasonic oscillations in aluminum compression tests and found that the flow stresses of the specimen were decreased. Daud *et al.*<sup>[2]</sup> also modeled their experiments using Abaqus/implicit and demonstrated that it was not sufficient to explain the effects of ultrasonic excitation in the metal forming processes only in terms of oscillatory stress superposition and contact friction. Their results suggest that it is necessary to understand the way ultrasonic energy is absorbed by aluminum in terms of its microstructure in

order to explain the benefits for a range of metal forming processes. Huang *et al.*<sup>[3]</sup> studied the influence of ultrasonic vibration on the hot upsetting of a model paste and found that applying a short longitudinal ultrasonic pulse to the die reduces the mean forming force during upsetting. Hung *et al.*<sup>[4]</sup> also got the same result for the ultrasonic vibration hot upsetting of an aluminum specimen. Marakawa *et al.*<sup>[5]</sup> applied a radial ultrasonic vibration on the dies in the wire drawing process and found that the ultrasonic vibration can improve the surface quality of the wires and increase the critical drawing speed. Bunget and Ngaile<sup>[6]</sup> have investigated the ultrasonic vibration-assisted forward and combined microextrusion with the billet diameter from 10 mm down to 0.5 mm and fabricated small parts with good surface quality. Ultrasonic vibration has also been applied in the sheet metal forming process. Jimma,<sup>[7]</sup> Ashida,<sup>[8]</sup> and Oliver<sup>[9]</sup> have done extensive research in this area and found that seasoning crack of the drawn cups could be avoided and the limited drawing ratio could be increased when ultrasonic vibration was applied.

It is believed that the benefits of using ultrasonic vibration in enhancing the metal forming processes are related to the reduction of friction forces between the die and the specimen and more importantly to the reduction of flow stresses in the material. The most common causes of the reduction of flow stress are as follows<sup>[1-4,10]</sup>: (1) dislocations might absorb energy through resonance and overcome slip obstacles; (2) the internal friction effect; and (3) the superposition of steady stress and alternating stress. Overall, the effects of ultrasonic vibration on metal forming are very complex.

On the other hand, ultrasonic vibration has been demonstrated to be capable of refining the microstructure and improving the mechanical properties of the

---

YANXIONG LIU, Lecturer, is with the Hubei Key Laboratory of Advanced Technology of Automotive Parts, Wuhan University of Technology, Wuhan, P.R. China, and also with the Department of Mechanical Engineering Technology, Purdue University, 401 North Grant Street, West Lafayette, IN 47906. SERGEY SUSLOV, Postdoctor, is with the Department of Material Engineering, Purdue University. QINGYOU HAN, Professor, is with the Department of Mechanical Engineering Technology, Purdue University. LIN HUA, Professor, is with the Hubei Key Laboratory of Advanced Technology of Automotive Parts, Wuhan University of Technology. Contact email: lhuasvs@yahoo.com.cn CLAUSE XU, Engineer, is with the Hans Tech, 3120 Bowfield way, West Lafayette, IN 47907.

Manuscript submitted October 30, 2012.

Article published online March 28, 2013

specimen.<sup>[11–18]</sup> Using single crystals, Belozeroval *et al.*<sup>[13]</sup> observed that the density of dislocations was increased with increasing time such that the specimen was exposed to high-intensity ultrasonic vibration. Langenecker and coworkers<sup>[17]</sup> found that a distinct cellular structure, about 2  $\mu\text{m}$  in size, was formed in ultrasonically treated aluminum nanocrystals after it was exposed to ultrasonic vibration for only 8 seconds. Liu *et al.*<sup>[19]</sup> combined the effect of the ultrasonic vibration and plastic deformation to refine the grains of solid pure copper and obtained grains in the range of 100 to 300 nm. The formation of such small grains in solid materials subjected to high-intensity ultrasonic vibration is believed to be related to the alignment of dislocations in a severely deformed specimen to form grain boundaries.

Most of the research in the area of superimposing ultrasonic vibration with metal forming processes has focused on the processing parameters and the quality of the specimen, while the influence of ultrasonic vibration on the microstructure has been largely ignored. The research on grain refinement of solid materials has been concentrated on small specimens subjected only to ultrasonic vibration. This present study focuses on combining the conventional upsetting (CU) process with high-intensity ultrasonic vibration to achieve extremely small grains and to evaluate the effect of ultrasonic vibration on the plastic deformation process and the microstructure formation.

Both ultrasonic vibration-assisted upsetting (UAU) and CU processes were carried out for a comparative study. For the UAU process, the ultrasonic wave was injected into the specimens directly. Through observing the microstructure of the samples obtained from these two forming processes using an optical microscope and transmission electron microscope, the effect of the ultrasonic vibration on the microstructure of the specimens during the plastic deformation process is discussed. Meanwhile, due to the fact that the phenomenon related to ultrasonic vibration occurs at a high frequency (20 kHz), the finite element method was used to analyze the difference between the UAU and the CU process, in terms of forming force, and metal flow.

## II. EXPERIMENTAL PROCEDURE AND THE FE MODEL

In order to investigate the effect of the ultrasonic vibration on the forming process and microstructure, the high-intensity ultrasonic vibration was injected directly into the specimen during the upsetting process. Figure 1 depicts the schematics for the UAU and CU process. For the UAU experiment, the specimen was connected with the horn tightly, and the entire setup was placed vertically on the die plate (shown in Figure 1(a)). For the CU experiment, the specimen was put vertically between two die plates; as the upper die plates moved down, the specimen deformed. During the UAU process, the height reduction of the specimen is about 4 mm. Therefore, to make the deformation in the same level, the displacement and the velocity of the upper die

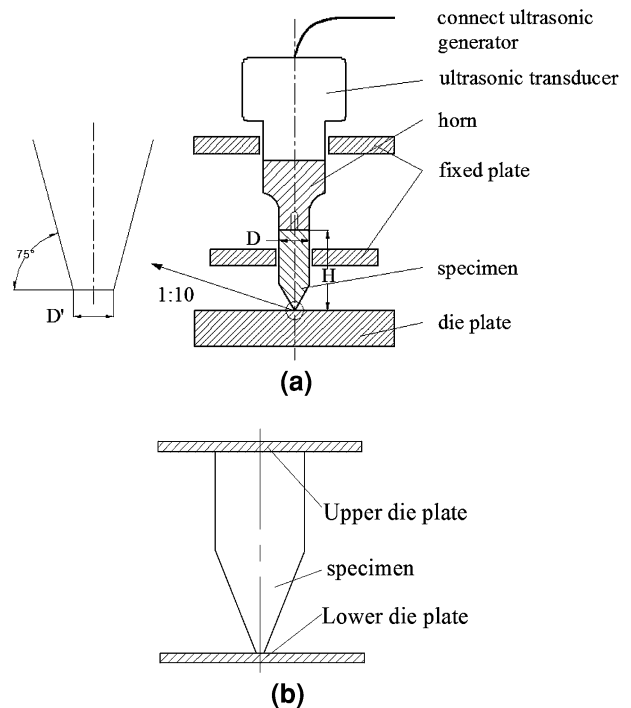


Fig. 1—Forming schematics: (a) ultrasonic-assisted upsetting process, (b) CU process.

plate of the CU process were set to 4 mm and  $0.1 \text{ mm s}^{-1}$ , respectively.

Commercial pure copper rods (99.99 wt pct), used in this study, were machined to conical tips (Figure 1(a)). The samples were then given an annealing heat treatment [973 K (700 °C) for 2 hours] to obtain a grain size of approximately 50  $\mu\text{m}$ .<sup>[19]</sup> The rod diameter  $D$  was 12.5 mm and the length of a specimen was 91 mm, which was equal to the half wave length of the ultrasonic wave traveling in the copper rod with a frequency of 20 kHz. This length was chosen in order to insure that the specimen resonated when the frequency of the ultrasonic transducer was 20 kHz. The tip diameter of the cone  $D'$  was in the range of 0.5 to 1 mm, carrying the total weight of the specimen and the ultrasonic unit (about 1.2 kg). The tip was in point contact with the steel substrate. Thus, a large external compressive stress was applied on the tip, insuring that the stress at the tip was largely compressive during ultrasonic vibrations. During the experiment, the contact area between the tip and die plate is variable. Therefore, only the initial compressive stress can be obtained, which is about 60 MPa. The UAU experiment was carried out at room temperature; high-intensity ultrasonic energy was injected into the specimen for 40 seconds and then severe plastic deformation occurred in the tip.

The grain structure of the deformed region in the tip was observed by optical microscopy (OM) after etching with a dilute reagent (5 g  $\text{FeCl}_3$ , 20 mL  $\text{HCl}$ , 100 mL water). The microstructure was also examined using a JEOL transmission electron microscope (TEM). The TEM samples were prepared from the top surface of the deformed region of the rod by the FIB (Focused Ion

Beam) lift-out method in an FEI NovaLab 200 FIB system. The initial thinning was performed under a voltage of 30 kV and a current of 0.3 nA. The final thinning was performed at a lower voltage and current (10 kV, 23 pA) to decrease the damage from Ga ion beam on the sides of the sample. To characterize the microstructure, TEM was carried out using an FEI Tecnai operated at 200 kV.

The FE simulation of the upsetting process was also performed in this study. Abaqus/explicit was used to analyze the forming process of the UAU and CU processes. The explicit dynamic analysis is computationally efficient for the analysis of large models with relatively short dynamic response times and for the analysis of extremely discontinuous events or processes, and can use a consistent, large-deformation theory model to undergo large rotations and large deformation. The explicit dynamics analysis is based upon the implementation of an explicit integration of the body motion equations using the central-difference integration rule. The explicit central-difference operator satisfies the dynamic equilibrium equations at the beginning of the increment,  $t$ ; the accelerations calculated at time  $t$  are used to advance the velocity solution to time  $t + \Delta t/2$  and displacement solution to time  $t + \Delta t$ . The dynamic equilibrium equation is given by Eq. [1]:

$$\mathbf{M} \cdot \dot{\mathbf{u}} = \mathbf{P} - \mathbf{I} \quad [1]$$

Therefore, the acceleration at the beginning of the increment is computed by

$$\dot{\mathbf{u}}|_{(t)} = (\mathbf{M})^{-1} \cdot (\mathbf{P} - \mathbf{I})|_{(t)} \quad [2]$$

The equations of motion for the body are integrated using the explicit central-difference integration rule and are expressed:

$$\dot{\mathbf{u}}|_{(t+\frac{\Delta t}{2})}^N = \dot{\mathbf{u}}|_{(t-\frac{\Delta t}{2})} + \frac{(\Delta t|_{(t+\Delta t)} + \Delta t|_{(t)})}{2} \ddot{\mathbf{u}}|_{(t)} \quad [3]$$

$$\mathbf{u}|_{(t+\Delta t)} = \mathbf{u}|_{(t)} + \Delta t|_{(t+\Delta t)} \dot{\mathbf{u}}|_{(t+\frac{\Delta t}{2})} \quad [4]$$

The FE model of these two processes is shown in Figure 2. Since the specimen was axial symmetric, a 2D axial symmetry model was created to simplify the FE model and to improve the computation speed. The key problem for this FE model was how to apply the ultrasonic wave. During the UAU experiments, the ultrasonic wave was injected into the specimen directly. Therefore, an even pulse pressure  $P_0 p(t)$  was exerted on the top surface of the specimen (shown in Figure 2), which is an effective way to model the ultrasonic wave propagation in the rod.<sup>[20]</sup> For the CU process, the extra pulse pressure was set to zero ( $P_0 = 0$ ). Moreover, no mass scaling was applied in this model. The application of mass scaling greatly reduces the computation precision because the speed of the ultrasonic vibration propagation in the rod is very high.

The FE model included only three parts: a rigid punch, a specimen, and a die plate. The punch and the die plate were modeled as analytically rigid and were not required to be meshed. Four-node bilinear quadrilateral plane strain with reduced integration and hourglass control elements (CPE4R) was applied to model the specimen. The frictional behaviors between the specimen and the rigid dies were all assumed to follow Coulomb's friction model, and the friction coefficient was considered to be 0.25. The total displacement of the rigid punch was 4 mm. The parameters of the UAU process and the material properties used in this model are summarized in Table I.

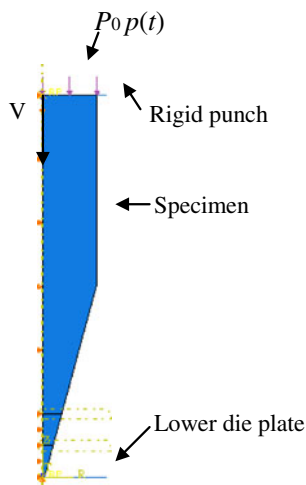


Fig. 2—2D FE model of the ultrasonic-assisted upsetting process.

**Table I. Summary of FE Model Parameters and the Material Properties**

Upsetting Speed, $V$ (mm s <sup>-1</sup> )	10
Frequency, $f$ (kHz)	20
$p(t)$	$\sin(125600t)$
$P_0$ (MPa)	23
Displacement of the Rigid Punch, $S$ (mm)	4
Density (kg m <sup>-3</sup> )	8960
Elastic Modulus $E$ (GPa)	119
Poisson's Ratio $\nu$	0.3
Plasticity	$\dot{\epsilon} = 2.983[\sin(0.0285\bar{\sigma})]^{3.752}$ $\exp(-205800/RT)$

### III. RESULTS

#### A. Metal Flow

Figure 3 depicts the final shape of the formed parts for the two forming processes: CU process (Figure 3(b)) and UAU process (Figure 3(d)). In order to compare the results of the experiments and the finite element analyses, the formed parts predicted using the FE method are also shown in Figure 3(a) for the CU process and in Figure 3(c) for the UAU process. The results illustrated in these images suggest that the finite element predictions are in good agreement with

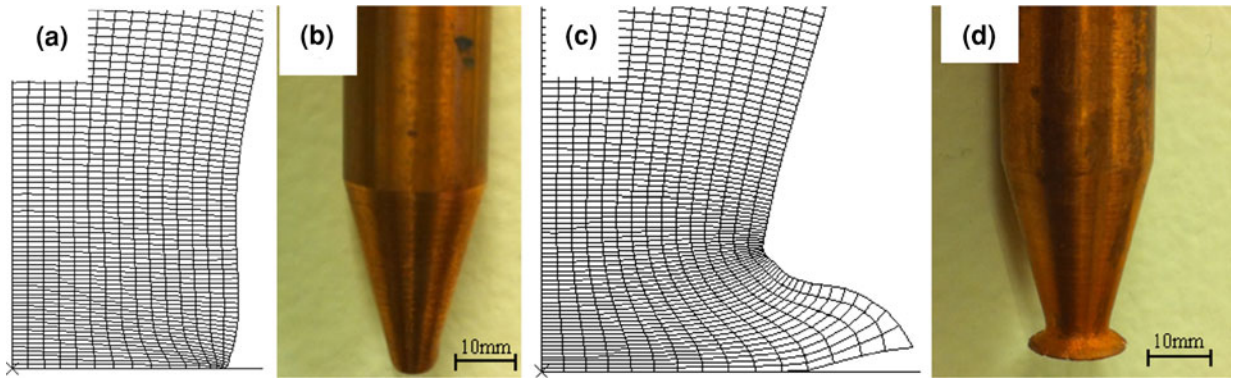


Fig. 3—Final shape of the formed parts: (a) predicted by FE and (b) by experiment for the CU process, (c) predicted by FE and (d) by experiment for the UAU process.

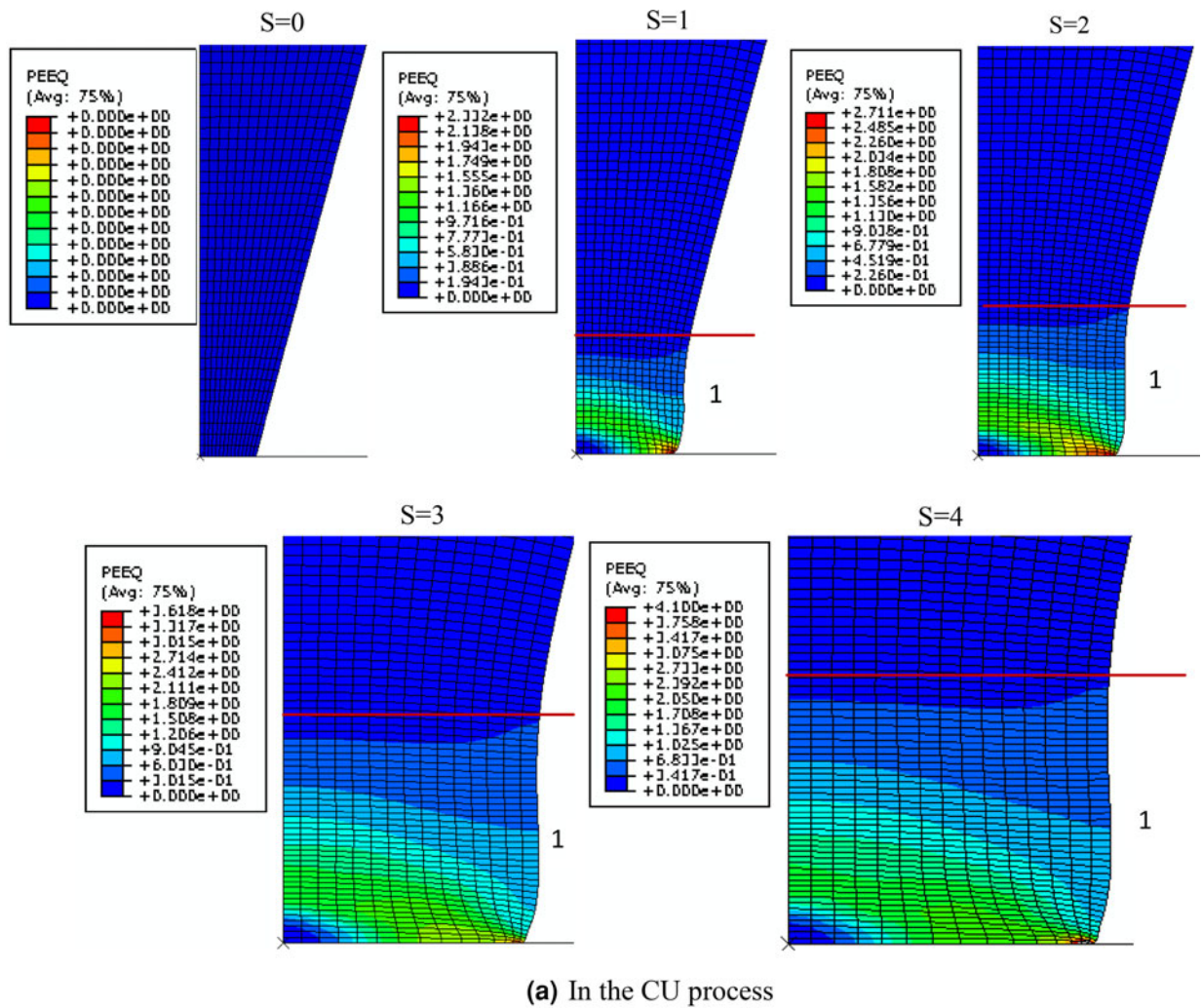
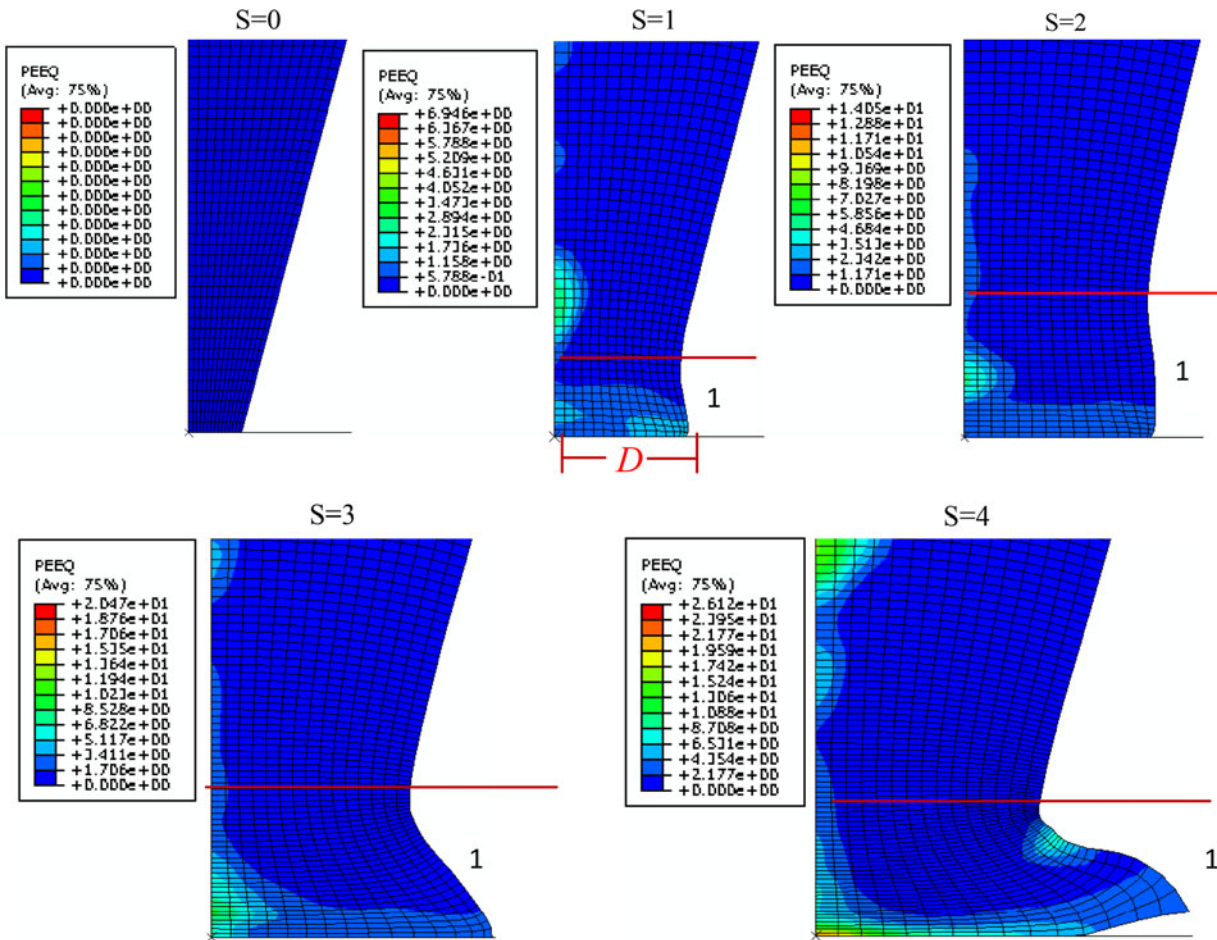


Fig. 4—Deformation characteristics for these two upsetting processes when the displacement is 1 to 4 mm.

experimental reality, indicating that the 2D FE model is valid. Results shown in Figure 3 also suggest that the metal flow for these two processes is quite different. Figure 4 shows the deformation process and equivalent plastic strain (PEEQ) step by step for both forming processes.

For the CU process (shown in Figure 4(a)), as the rigid punch moves down, the small tip deforms slightly when the displacement is 1 mm. Due to the friction force existing between the surfaces of the specimen and the lower die plate, the center of the tip is very hard to deform. The “drum effect,” as the main characteristic of



(b) In the UAU process

Fig. 4—continued.

the convention upsetting process, can be observed in the whole deformation process. With the increase of the height reduction of the specimen, the main deformation area (marked in Figure 4 with the number 1) only becomes larger in the radial direction. The maximum diameter of the tip  $D'$  was increased to 4.5 mm.

When the ultrasonic vibration is applied, no “drum effect” and hard deformation area can be observed during the forming process. As the punch moves down, the metal flows from the center to the edge area. The sharp end of the conical specimen was seriously deformed and looked like an umbrella. The diameter of the tip  $D'$  has been increased from 0.5 mm (the initial cone diameter) to 6.2 mm, indicating that severe plastic deformation occurred on the tip of the conical specimen. The reason for the difference of the metal flow for these two forming process will be discussed in Section IV.

### B. Forming Force

Figure 5 shows the forming force during both processes. For the CU process, the force–displacement variation curve is very typical. At first, the force

increased sharply, and then the force increased smoothly with the increase in displacement.

For the UAU process, the force is increased with the displacement during the forming process. However, from this figure, it is found that sometimes the forming force is zero and sometimes it is not. When the forming force is not zero, it is a little larger than that of the CU process. In this paper, the frequency of the ultrasonic vibration is 20 kHz. Although it would be best to save the analysis data in every cycle of the ultrasonic exciting, which is about 5e to 5s, if the time interval for the data saving is less than 5e to 5s, the final result data file will be very large and the simulation time will be very long. Therefore, just a very short interval, from the displacement of 0.1601 to 0.16224 mm, was selected to do the analysis as shown in the small window in Figure 5. From the selected displacement interval, we can find that the force changed sinusoidally with increasing displacement.

### C. Microstructure

The cross-sectional optical micrographs of the main deformation area of the specimens from both forming

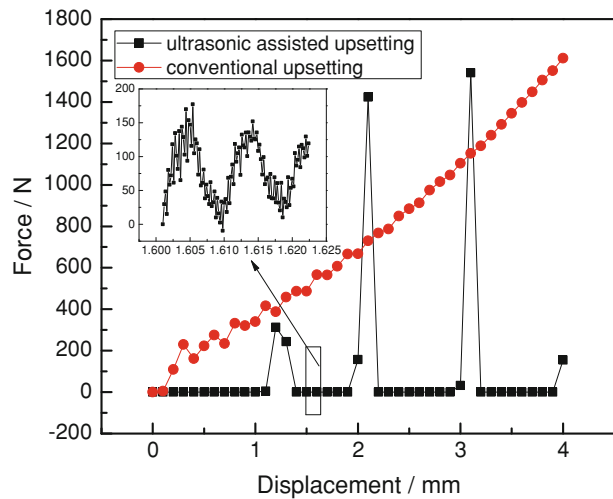


Fig. 5—Forming force versus the displacement for these two forming processes.

process are presented in Figure 6. At low magnification (Figures 6(a) and (b), 50 $\times$ ), the metal flow tracks can be seen clearly, which have good agreement with the results of the FE simulation (Figure 4). Figures 6(c) and (e) show the microstructures in the center and edge areas, respectively, of the CUed specimen as marked in Figure 6(a). The grain size in the center area of the CUed specimen is about 30 to 40  $\mu\text{m}$ , and in the edge area, the grain size is about 10  $\mu\text{m}$ . Due to the hard deformation area being located in the center of tip close to the lower die plate, the grain only deformed slightly. The grain size in the edge area (Figure 6(e)) is much smaller than that in the center area. For the UAU process, the metal flows from the center to the edge and curves upward. Figures 6(d) and (f) present the microstructures in the center and edge areas, respectively, as marked in Figure 6(b). In the center area, the specimen impacts the lower die plate with a high speed during the forming process. Therefore, the grains have been greatly flattened under the action of the stress in the axial direction ( $\sigma_z$ ). The height of the severely deformed layer (marked in Figure 6(d)) is about 150  $\mu\text{m}$ . When the metal flows away from the center, it will be warped and separated from the lower die plate. However, by just using the optical microscope, it is very difficult to observe the grain structure of the UAUed specimen due to the grain size being in the nanoscale. Hence, to reveal the microstructure much more clearly, the specimens were tested by TEM methods.

Figures 7(a) and (b) depict the microstructures of the UAUed sample's center and edge areas (as marked in Figure 6(b)), respectively. The samples used for TEM were obtained from the cross section (paralleled to the loading direction) adjacent to the bottom surface of the tip. As illustrated in Figure 7, the copper grains have been greatly refined. The initial grain size of the specimen is  $\sim 50 \mu\text{m}$ , and then the grains have been refined to about 100 to 300 nm after the UAU process. Moreover, the difference of microstructures in the edge and center areas can be seen clearly from the TEM

images. In the center area (Figure 7(a)), only the dislocation cells and subgrains can be found. The neighboring dislocation cells are separated by dislocation walls. From the SAED pattern, the diffraction spots are diffuse, indicating that no high angle grain boundaries were obtained between neighboring grains.

In the edge area (Figure 7(b)), the grain boundary is very clear. Some equiaxed grains with the size of  $\sim 150 \text{ nm}$  near the bottom surface of the tip can be found. Far away from the bottom surface, the grains have been elongated in a band structure and subgrains existed within each grain. These grain bands lie approximately perpendicular to the press direction. The SAED pattern exhibits diffracted beams scattered around rings, thus indicating that the grain boundaries have high angles of misorientation.

Comparing the microstructures of the specimens from Figures 6 and 7, it is clearly found that the grains produced by the UAU process are much smaller than those by the CU process. The grains have been severely refined to the nanoscale after the UAU process. However, the grain deformed slightly during the CU process. This means that the ultrasonic vibration can make the specimen's plastic deformation much more severe and improve the grain refinement efficiency.

## IV. DISCUSSION

### A. UAU Process Deformation Mechanism

The deformation mechanism of the ultrasonic vibration-assisted metal forming is different from the conventional forming process. In the published research on the application of ultrasonic vibration in the metal forming process, almost all of the ultrasonic vibration was exerted to the die plates, *e.g.*, the ultrasonic vibration extrusion and ultrasonic vibration upsetting presented by the authors Mousavi and Hung,<sup>[4,20]</sup> respectively. In these experiments, the die plate would be vibrated sinusoidally with a frequency of 20 kHz. The schematics of ultrasonic vibration application in their experiments are shown in Figure 8.

During the CU process, the lower die is stationary. With the movement of the upper die, the billet is deformed. Therefore, the actual extrusion speed is equal to the velocity of the upper die movement. However, in the ultrasonic vibration upsetting process (Figure 8(b)), the die was sinusoidally vibrated along the axial direction during the forming process. In this case, the actual speed is different from the conventional one.

For the UAU process, the ultrasonic wave was applied on the top surface of the billet as shown in Figure 1. When the wave is transmitted in the specimen, the particles of the solid will be vibrated. In our experiments, the input ultrasonic wave was sinusoidal, so the particles on the bottom surface of the tip vibrated sinusoidally. Based on the theory about the relationship between the active force and the reactive force, the effect of the particles' vibration at the bottom surface is the same as the vibration of the die plate. Therefore, the velocity analysis about the ultrasonic vibration upsetting

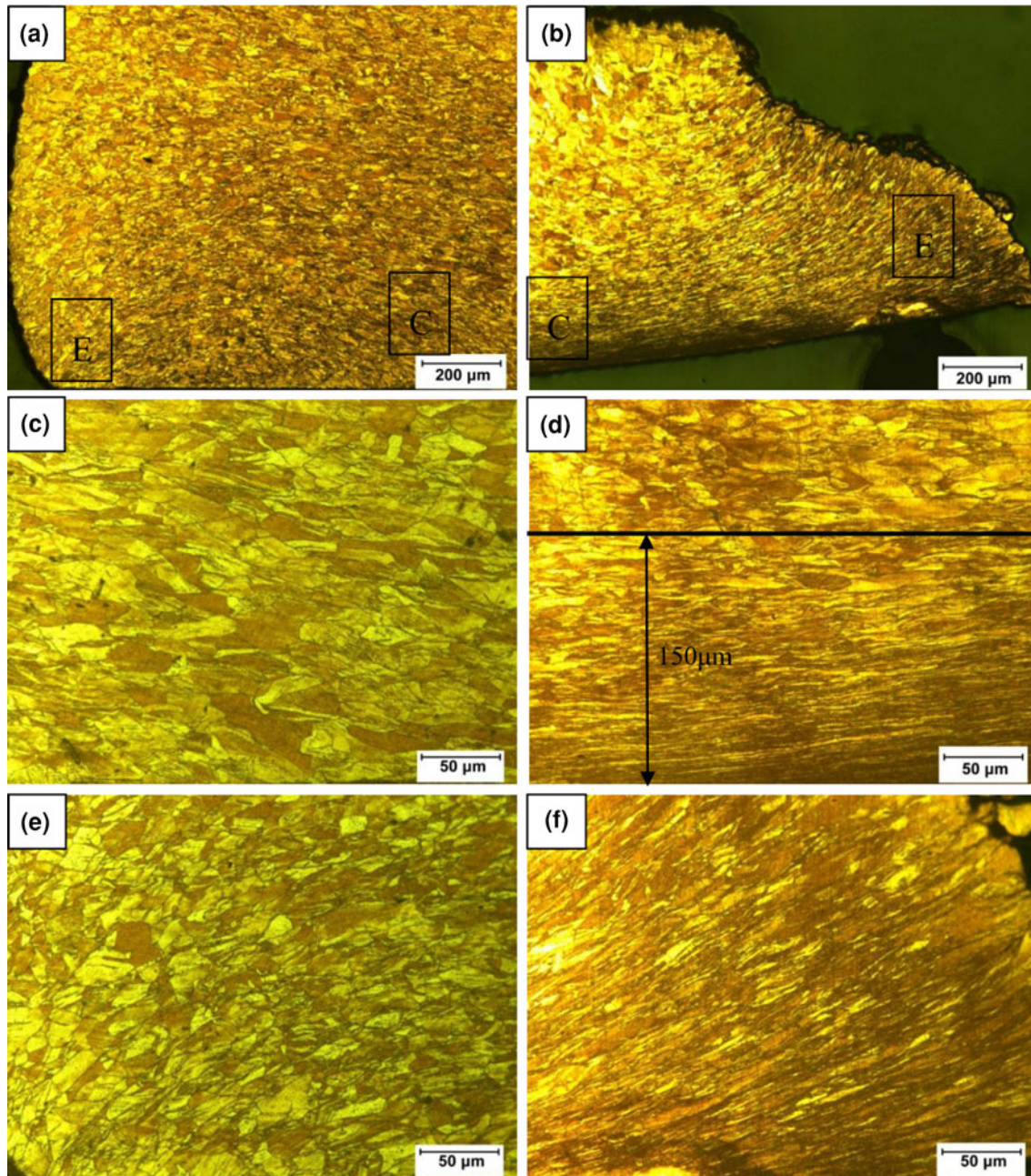


Fig. 6—Cross section metallographic images of the main deformation region of the CUed sample and UAUed sample. (a) CUed sample (50×), (b) UAUed sample (50×), center area of the CUed sample (c) and UAUed sample (d) (200×), edge area of the CUed sample (e) and UAUed sample (f) (200×).

presented by Mousavi<sup>[21]</sup> can also be applied in this paper to illustrate the deformation mechanism of the UAU process.

During the ultrasonic vibration upsetting process, the actual (relative) speed ( $V_{rel}$ ) can be separated into two parts, apparent extrusion speed ( $V_e$ ) and the die axial vibration speed ( $V_{au}(t)$ ), and these velocities have to obey Eq. [5].

$$\vec{V}_{rel} = \vec{V}_e + \vec{V}_{au}(t) \quad [5]$$

Figure 9 shows the schematics of the velocity and displacement variations versus time. We assumed that

the die vibration can be expressed as  $S = a \sin(\omega t + b)$ , and the velocity of the vibration  $V_{au}(t) = \frac{\partial S}{\partial t} = a\omega \sin(\omega t + b)$ . Therefore, the maximum die vibration speed would be  $V_{au}(t)_{max} = a\omega = 2\pi af$ ,  $a$  and  $f$  being the amplitude and the frequency of vibration, respectively. If the extrusion speed is less than the maximum vibration speed ( $V_{e1} < V_{au}(t)_{max}$ , as shown in Figure 9(a)), the die shoulder could be separated from the billet (the corresponding displacement of the punch at a speed of  $V_{e1}$  is  $S_{e1}$ , as shown in Figure 9(b)). As shown in Figure 9(b), during the time interval between  $t_1$  and  $t_2$ , the die shoulder will separate from the billet and a gap will be created between the die shoulder and the

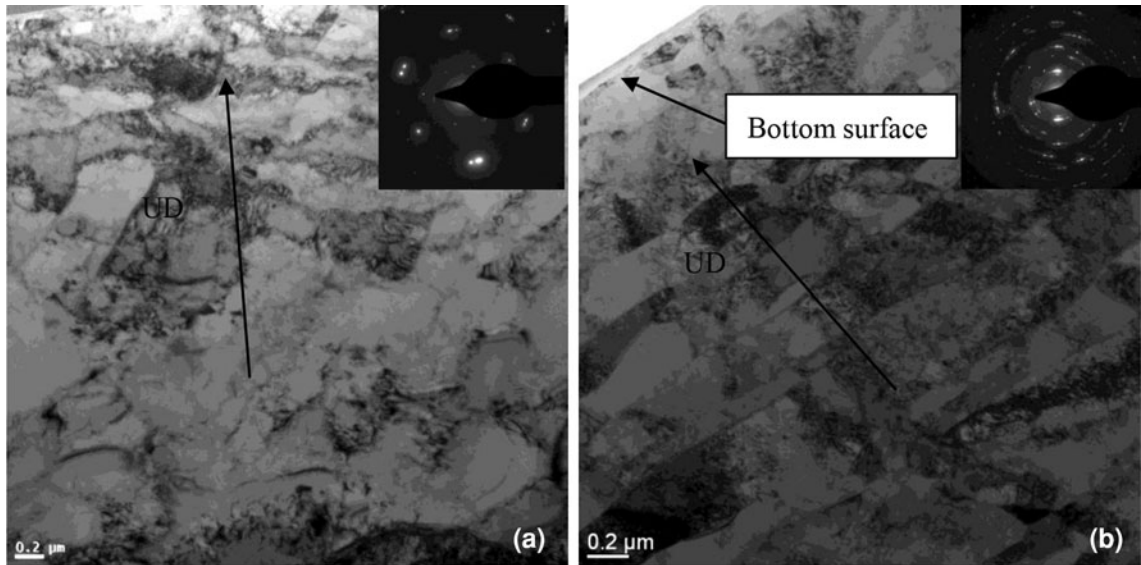


Fig. 7—TEM images of the UAUed sample from (a) center and (b) edge area.

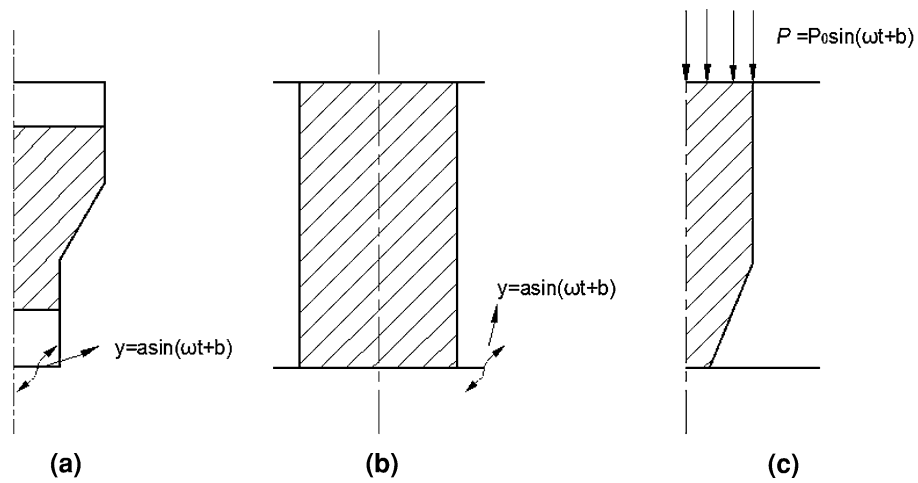


Fig. 8—Schematics of the ultrasonic vibration application: (a) ultrasonic vibration extrusion<sup>[21]</sup>; (b) ultrasonic vibration upsetting<sup>[3]</sup>; (c) ultrasonic-assisted upsetting in this paper.

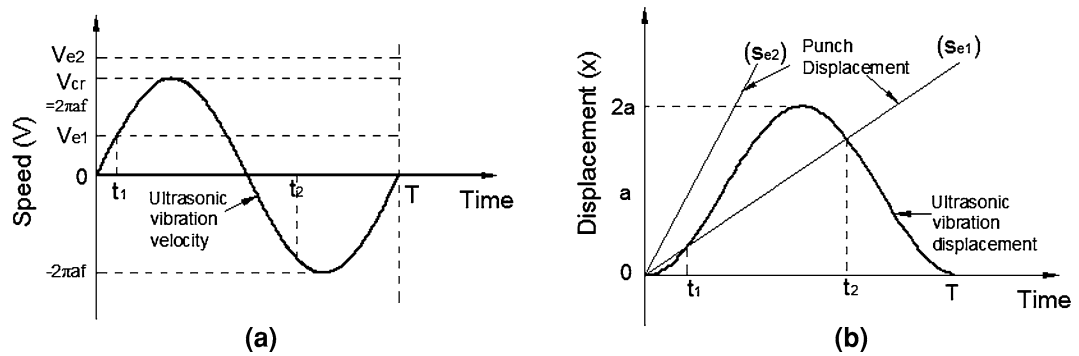


Fig. 9—Schematics of the velocity and displacement variations versus time in a cycle: (a) variations of extrusion and vibration speed; (b) variations of punch and die vibration displacement.



material. Moreover, if the upsetting speed is higher than the maximum vibration speed ( $V_{e2} > V_{au}(t)_{\max}$ , as shown in Figure 9(a)), the displacement of the punch is always larger than that of the die vibration. Therefore, the die shoulder cannot separate from the billet and the critical extrusion speed is  $V_{cr} = 2\pi af$ .

In this paper, with the help of the FE simulation, the vibration amplitude of the particle at the bottom surface with different pulse pressure  $P_0$  (Figure 2) can be obtained. When the pulse pressure  $P_0$  is 23 MPa, the amplitude is about  $22.5 \mu\text{m}$ , which is the same as the amplitude of the specimen vibration in the experiment. Therefore, according to the speed analyses mentioned above, the  $V_{cr} = 2\pi af = 2826 \text{ mm s}^{-1}$ . The upsetting speed set in this study is  $10 \text{ mm s}^{-1}$ , which is much smaller than  $V_{cr}$ . Therefore, the specimen will be separated from the die plate at some of the time. The force–displacement history curve (Figure 5) also proved this point.

During the UAU process, the specimen contacted with and separated from the die plate in every cycle; in other words, the specimen impacted the rigid die plate 20,000 times per second. Therefore, the UAU process deformation mechanism is high frequency impacting. After processing by the high frequency impacting process, an aluminum cylinder workpiece has been severely deformed with “reverse drum effect”<sup>[22]</sup> (“Drum effect” is the main characteristic for the CU). A similar phenomenon was also observed during the Taylor impacting test.<sup>[23]</sup> When a steel rod impacted a rigid boundary with a high speed ( $\sim 100 \text{ m s}^{-1}$ ), severe plastic deformation occurred at the rod impact end and the shape of the end of the rod looks like as an umbrella. This phenomenon is associated with the superposition of the elastic wave and the plastic wave.<sup>[24]</sup> However, the temperature induced during the impacting process should also be taken into account for this problem.

Ultrasonic wave is a kind of mechanical energy.<sup>[11]</sup> When it transmits into a solid material, a part of the energy will be absorbed and dissipated due to physical processes such as thermoelastic (or heat) losses, dislocation internal friction, magnetomechanical loss, and so on.<sup>[25]</sup> Then, this part of energy will be converted into heat. By analyzing the mechanism of heat conduction absorption with account for the adiabatic character of heating and isobaric heat transfer, it is possible to obtain an expression for the coefficient of absorption  $\alpha_1$  (longitudinal waves in a rod)<sup>[16]</sup>:

$$\alpha_1 = \frac{\omega^2}{2\rho c_1^3} \left[ \left( \frac{4}{3}\mu' + \lambda' \right) + \frac{k_t T \alpha_T^2 c_1^2}{C_p^2} \left( 1 - \frac{4c_t^2}{3c_1^2} \right)^2 \right] \quad [6]$$

where  $\omega$  is the frequency,  $\rho$  is the material density,  $c_1$  and  $c_t$  are the velocity of the longitudinal and shear waves, respectively,  $\mu'$  and  $\lambda'$  are the imaginary parts of the first and second Lamé constants, respectively,  $k_t$  is the heat conductivity,  $\alpha_T$  is the coefficient of thermal expansion, and  $C_p$  is the heat capacitance at constant pressure. The specific values of the physical properties for copper are<sup>[26]</sup>  $\rho = 8960 \text{ kg m}^{-3}$ ,  $c_1 = 3810 \text{ m s}^{-1}$ ,  $c_t = 2325 \text{ m s}^{-1}$ ,

$\mu' = 45 \text{ GPa}$ ,  $\lambda' = 95 \text{ GPa}$ ,  $k_t = 401 \text{ W m}^{-1} \text{ K}^{-1}$ ,  $\alpha_T = 16.5 \mu\text{m m}^{-1} \text{ K}^{-1}$ , and  $C_p = 24.44 \text{ J mol}^{-1} \text{ K}^{-1}$ .

Using the above values, and substituting them into Eq. [4], one gets  $\alpha_1 = 0.311$ .

Therefore, the temperature increased during the UAU process can be obtained by this equation:

$$\Delta T = \frac{\alpha_1 W t}{cm}, \quad [7]$$

where  $W$  is the power of the ultrasonic generation,  $t$  is the process time,  $c$  is the specific heat, and  $m$  is the mass of the specimen.

For our case,  $W = 1.5 \text{ kW} \cdot 0.6 = 900 \text{ J s}^{-1}$ ,  $t = 40$  seconds (the UAU processing lasted for 40 seconds),  $c = 0.385 \text{ J g}^{-1} \text{ }^\circ\text{C}^{-1}$ ,  $m = 124 \text{ g}$ . Substituting these values into Eq. [5], we get the increased temperature during the UAU forming process as about  $507 \text{ K}$  ( $297 \text{ }^\circ\text{C}$ ).

The heat generation during the ultrasonic vibration forming process has also been observed by the other researchers. Using the method of infrared radiometry, Langenecker *et al.*<sup>[27]</sup> revealed the temperature profile, the heating rate, and the absolute energy absorption during ultrasonic propagation. The research showed that about 50 percent of the total electrical power input to the transducer was converted to heat within the hot zone of the sample. Other research, such as made by Kristoffy,<sup>[28]</sup> Rozner,<sup>[29]</sup> Adams *et al.*,<sup>[30]</sup> Huang *et al.*,<sup>[2]</sup> and so on, illustrated that the ultrasonic vibration can increase the specimen's temperature. In our experiments, during the ultrasonic vibration upsetting, severe heat was generated. In order to avoid the temperature from being too high to make the grains grow rapidly,<sup>[31]</sup> cold water [ $298 \text{ K}$  ( $25 \text{ }^\circ\text{C}$ )] was used as a coolant during the forming process. The temperature at the cone tip was kept around  $373 \text{ K}$  ( $100 \text{ }^\circ\text{C}$ ) during the UAU experiments.

In hot deformation studies, it is generally observed that the steady state flow stress, strain rate, and temperature obey a kinetic rate equation<sup>[32]</sup>:

$$\dot{\epsilon} = A \sigma^n \exp \left[ \frac{-Q}{RT} \right], \quad [8]$$

where  $A$  is a constant,  $n$  is the stress exponent,  $Q$  is the activation energy, and  $R$  is the gas constant. Equation [6] illustrated that the strain rate increased with the increasing of the temperature when the stress is in a certain value. Therefore, with the temperature rise during the UAU process, the pure copper conical tip deformed much more severely than that in the CU process.

## B. Grain Refinement Mechanism

The pure copper grains with the initial size of  $\sim 50 \mu\text{m}$  were refined to about 100 to 300 nm after a one time UAU forming process. This is the result of the severe plastic deformation (SPD), which has been widely applied to produce the bulk ultrafine-grained (UFG) materials. The average grain size achieved in pure metals

using various conventional SPD techniques, such as equal channel angular pressing (ECAP), high pressure torsion (HPT), and so on, usually lies in the range of ~150 to 300 nm.<sup>[33]</sup> Thus, the UAU process could be another effective process of SPD to produce UFG materials.

During the UAU process, the metal just flowed from the center to the edge area; therefore, we can get the microstructure evolution process by observing the microstructure in the center and edge areas. Figures 10(a) and (b) show the microstructures in the center and edge areas, respectively. As marked in Figure 10(a), many dislocations have been arranged and dislocation cells can be found in a grain. These dislocations cells separated by dense dislocation walls (DDWs) subdivide the original grains into regions. During the grain refinement process, the individual grains of polycrystalline metals are subdivided into cell blocks.<sup>[34–36]</sup> These cell blocks in turn are subdivided into ordinary dislocations cells and microbands. However, the reorientation is different among neighboring dislocation cells.<sup>[37]</sup> Thus, under the action of shear stress, these dislocation cells rotate with each other, and then the misorientation between the dislocation boundaries increases steadily.<sup>[38]</sup> Finally, grains with high angle grain boundary are obtained as shown in Figure 10(b). It is apparent from Figure 10(b) that these dislocation cells were evolved into equiaxed micrograins under the action of shear stress caused by the metal flow from the center to the edge. The shape of the equiaxed grain is hexagonal, which has a good agreement with the predicted shape made by Meyers and coworkers.<sup>[39,40]</sup>

As shown in Figure 10(b), equiaxed grains only exhibited around the bottom surface. Far away from the bottom surface, lots of elongated subgrain bands were observed. These subgrain bands appear to be the precursor of the well-defined equiaxed grains.<sup>[41]</sup> In the UAU process, the bottom surface hit the plate with a high frequency, and much more severe strain was

imposed on the grains in this region. These elongated structures were seen in many metals subjected to high strains, as reported by, *e.g.*, Gil Sevillano *et al.*<sup>[42]</sup> Hughes and Hansen<sup>[37]</sup> reported rotations of 30 to 40° at medium and large strains (cold rolling reductions from 70 to 90 pct). Similar observations and analyses were made by Hansen and coworkers.<sup>[43–46]</sup>

It is well known that when the subgrains with a low angle boundary transfer to the equiaxed grain with a larger angle boundary, the misorientation between the neighbor grains will be increased. During this process, the grains should be rotated against each other to increase the misorientation.<sup>[35]</sup> The rotation of the grains is dependent on the stress state during the deformation process. Figure 11 shows the stress state for the UAUed specimen. Volume elements with the width of  $dr$  from the center and the edge areas were selected for the stress analysis. The stress component of the volume element is depicted in Figure 11. The volume element suffers axial stress  $\sigma_z$  (paralleled to the loading direction), radial stress  $\sigma_r$ , tangential stress  $\sigma_\theta$ , and shear stress  $\tau$ . In the center area, the axial stress  $\sigma_z$  is very large due to the center area impacting the lower die plate with a high speed during the forming process. The axial stress  $\sigma_z$  is so large that the other stress will have a small or no effect on the element deformation. Therefore, the grains are very hard to rotate and no large angle grain boundary is produced in the center area. However, in the edge area, the axial stress  $\sigma_z$  decreased sharply when the metal warped and separated from the lower die plate. Hence, the grains in this area can be rotated easily under the action of the shear stress and grains with large angle boundary can be obtained.

### C. Effect of the Ultrasonic Vibration in the Grain Refinement

The ultrasonic vibration can make the specimen's plastic deformation much more severe and help to

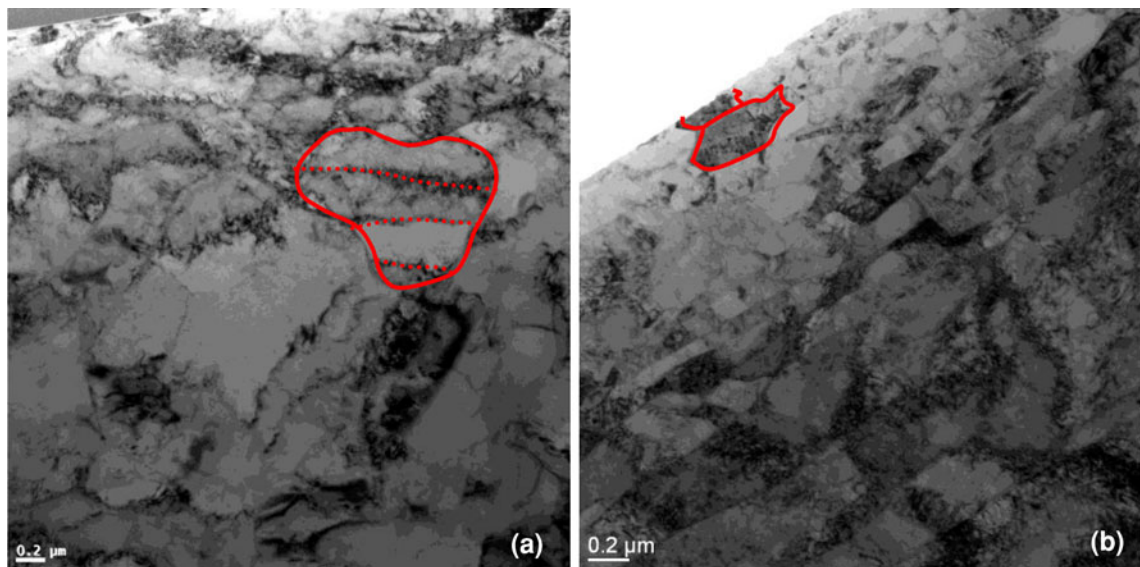


Fig. 10—Microstructure evolution during the ultrasonic vibration upsetting: (a) in the center area and (b) in the edge area.

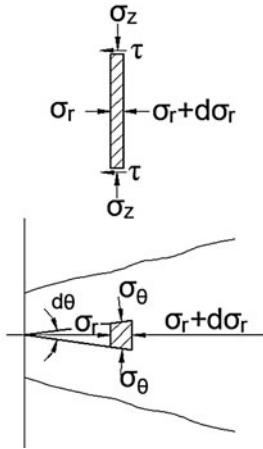
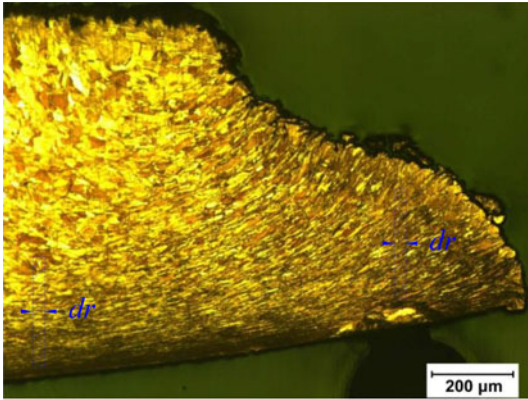


Fig. 11—Stress state analysis for the selected area of the UAUed specimen.

improve the grain refinement efficiency when it transmits in the specimen. Several facts should be considered for this phenomenon, and they are presented as follows.

### 1. Stress superposition

When the ultrasonic wave transmits in the solid it can disturb the particles of a body from equilibrium, which gives rise to internal forces that tend to return these particles to equilibrium. These internal forces per unit area are known as stresses. The stresses associated with the propagation of ultrasonic wave are the basic cause of the numerous mechanical effects attributable to improving the material microstructure.<sup>[11]</sup>

The stress produced by an ultrasonic wave traveling through a solid may be calculated from References 47, 48:

$$s = \xi \rho \omega c, \quad [9]$$

where  $\xi$  is the particle displacement,  $\rho$  is the density,  $\omega$  is the angular frequency, and  $c$  is the wave velocity in the specimen.

In this study,  $\xi = 22.5 \mu\text{m}$ ,  $\rho = 8960 \text{ kg m}^{-3}$ ,  $\omega = 125,600 \text{ Hz}$ , and  $c = 3644.3 \text{ m s}^{-1}$ .

Therefore, the stress caused by the ultrasonic vibration  $s = 92.2 \text{ MPa}$ . But, the yield stress for the annealed copper is only about  $70 \text{ MPa}$ . In our experiments, no plastic deformation occurred if only the

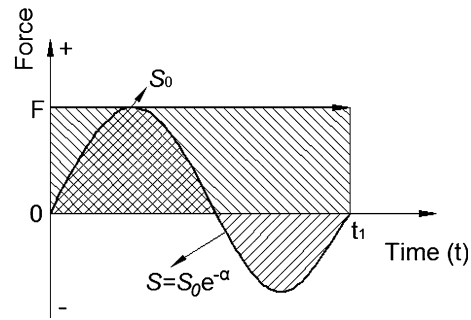


Fig. 12—Impulse  $I$  of the particle changing with the time.

ultrasonic wave was applied in the specimen. Therefore, the stress predicted by Eq. [2] is a little larger than that in reality due to it being an empirical equation. However, we can still conclude that the stress is very large and even close to the yield stress of the material.

The effect of the extra force on the plastic deformation is discussed here. The plastic deformation is caused by the dislocation slip for the copper. It is assumed that a constant force  $F$  is acted on a particle with the weight of  $m$ , and then an extra force  $S$  which changed sinusoidally is exerted on it. Due to the attenuation of the ultrasonic wave dissipation, the force  $S = S_0 e^{-\alpha}$ , where  $\alpha$  is the coefficient of absorption.<sup>[16]</sup> The impulse of the mass,  $I = Ft$ , changing with time is shown in Figure 12. According to the Momentum theorem  $Ft = m \cdot \Delta v$ , the velocity of the particle is  $\Delta v = Ft/m$ . The impulse  $I$  is a vector. From Figure 12, the total impulse caused by the extra force  $S$  is positive. Therefore, the extra force  $S$  can speed up the movement of the particle.

From the view of the grain boundary rotation, the extra force  $S$  can also make it much easier for rotation to occur. A simple model can be used to estimate the driving force to maintain an equiaxed structure, which is obtained by equating the force acting on a curved segment of  $dS$  due to the grain boundary energy,  $\gamma$ . The velocity of the grain boundary is proportional to the force acting on the segment  $dS$ <sup>[49]</sup>:

$$v \propto \frac{\gamma}{R} = S \quad [10]$$

Due to the superposition of the extra force  $S$ , when the ultrasonic wave transmits in the solid, the driving force acting on the grain boundary will be increased. From Eq. [3], the larger the driving force, the bigger the grain boundary rotation velocity.

### 2. Dislocation movement

The ultrasonic vibration can push dislocation to be moved. A linear dislocation can vibrate under the action of a cyclic mechanical stress like a string imposed by forced vibrations.<sup>[50]</sup> Inspired by this idea, a much more impeccable model was created.<sup>[51]</sup> It is assumed that dislocations are linear and pinned with interstitial atoms, point defects, and dislocation network nodes.

The pinning of dislocations with network nodes is superior to that with point defects and interstitials. Pinning with point defects controls the dislocation loop length  $L_P$  which is smaller than the loop length  $L_N$  between dislocation network sites. In the range of very weak stresses, the dislocation loops  $L_P$  bow and break away when a particular stress level is achieved, which is accompanied by an abrupt increase in the dislocation loop length from  $L_P$  to  $L_N$ . Once a break stress is surpassed, the dislocation strain dramatically increases, which results in a bowing of the loop  $L_N$ . The network nodes are assumed to be extremely strong at locking points, allowing no breakaway to occur. A further increase in the applied stress leads to the excitation of the Frank-Read sources and, hence, to plastic strain.

Many experiments have been carried out to analyze the effect of ultrasonic vibration on material structures, and the results have proved that the above model is correct. Pines *et al.*<sup>[52]</sup> pointed that the dislocation density grew with the time of ultrasonic treatment, first linearly, but then went into a plateau. The saturation density of dislocations was linearly dependent on temperature. Langenecker and coworkers<sup>[48,53]</sup> showed that ultrasonic treatment acted to increase the density of dislocations and their wall-like alignment. They directly observed the reproduction of dislocations under the action of 40 kHz ultrasonic vibrations excited in the specimen. Therefore, the ultrasonic vibration can make the plastic deformation occur in an easier manner.

### 3. Temperature

As mentioned before, the temperature rose during the UAU process. The temperature has a great effect on the boundary rotation. The higher the temperature, the easier the grain boundary rotation. When the temperature is  $0.5T_m$  (it is about 677 K for copper), a grain rotation of 30 deg takes place in less than 1 ms, while with decreasing temperature, this rotation takes progressively longer.<sup>[39,40]</sup> In the UAU experiments, the temperature at the cone tip was kept around 373 K (100°C). The CU experiments were carried out at the room temperature. Therefore, the heat induced during the UAU process can increase the grain boundary surface energy and make the grain boundary rotation much easier.

## V. CONCLUSIONS

The paper presented here explores the difference between the CU and UAU processes and reveals the deformation mechanism and the microstructure revolution mechanism of the UAU process. In order to achieve this goal, the upsetting experiments with and without ultrasonic vibration were carried out, and the FE method was applied to analyze the forming process due to the ultrasonic vibration processing phenomenon occurring at high speeds. From this study, we arrived at the following conclusions:

1. Metal flow for these two forming processes is completely different. The plastic deformation for the

UAU process is much more severe than that of the CU process. The sharp end of the tip specimen produced by the UAU process looked like an umbrella, and no “drum effect” was found even though it is the main deformation characteristic of the CU process.

2. The deformation mechanism for the UAU process is as follows: During the upsetting process, the specimen will separate from the die plates due to the upsetting velocity being smaller than the critical speed  $V_{cr} = 2\pi af$ . The UAU process deformation mechanism is high frequency impacting. The deformation characteristic is discussed in this paper for the high frequency impacting problem.
3. The pure copper grains with initial grain size 50  $\mu\text{m}$  were refined to 100 to 300 nm by the UAU process. The grain refinement mechanism is discussed, and the reasons for the difference of the microstructures between the center and edge areas of the UAEd sample were understood.
4. The reasons why the ultrasonic vibration can improve the grain refinement efficiency were discussed. The reasons are the superposition stress caused by the ultrasonic vibration, the dislocation movement, and the heat generation caused by the ultrasonic wave propagation in the solid.

## ACKNOWLEDGMENTS

The authors would like to thank the National Basic Research Program of China (No. 2011CB706605) and the Innovative Research Groups of the National Natural Science Foundation of Hubei Province (No. 2011CDA122) for the support given for this research project.

## REFERENCES

1. Y. Daud, M. Lucas, and Z. Huang: *Ultrasonics*, 2006, vol. 44, pp. 511–15.
2. Y. Daud, M. Lucas, and Z. Huang: *J. Mater. Process. Technol.*, 2007, vol. 186, pp. 179–87.
3. Z. Huang, M. Lucas, and M.J. Adams: *Ultrasonics*, 2002, vol. 40, pp. 43–50.
4. J.C. Hung and C. Huang: *Ultrasonics*, 2005, vol. 43, pp. 692–70.
5. M. Murakawa and M. Jin: *J. Mater. Process. Technol.*, 2001, vol. 113, pp. 81–90.
6. C. Bunget and G. Naile: *Ultrasonics*, 2011, vol. 51, pp. 606–17.
7. T. Jimma, Y. Kasuga, and N. Iwaki: *J. Mater. Process. Technol.*, 1998, vols. 80–81, pp. 406–12.
8. Y. Ashida and H. Aoyama: *J. Mater. Process. Technol.*, 2007, vols. 187–188, pp. 118–26.
9. K.C. Oliver, C. Hansen, and P. Knoll: *Ultrasonics*, 2004, vol. 42, pp. 989–96.
10. A.E. Eaves, A.W. Smith, W.J. Waterhouse, and D.H. Sansome: *Ultrasonics*, 1975, vol. 7, pp. 162–69.
11. D. Ensminger and F.B. Stulen: *Ultrasonics-Data, Equations, and Their Practical Uses*, 2nd ed., CRC Press, New York, 2009, p. 620.
12. E.G. Shvidkovshii, N.A. Tyapunina, and E.P. Belozero: *Kristallografiya*, 1962, vol. 473, pp. 7–15.
13. E.P. Belozero, N.A. Tyapunina, and E.G. Shvidkovskii: *Kristallografiya*, 1963, vol. 232, pp. 8–16.

14. I.G. Polotskii, D.E. Ovsienko, and E.L. Khodov: *Met Metalloved*, 1967, vol. 744, pp. 23–31.
15. I.G. Polotskii, G.I. Prokopenko, and V.I. Trefilov: *Tverd Tela*, 1969, vol. 155, pp. 11–21.
16. O.V. Abramov: in *High-Intensity Ultrasonics: Theory and Industrial Applications*, Kurnakov Institute of General and Inorganic Chemistry, Moscow, 1998, p. 98.
17. B. Langenecker: *IEEE Trans. Sonics Ultrasonics*, 1966, vol. 13, pp. 1–8.
18. A.V. Kulemin: *Ultrasound and Diffusion in Metals*, Metallurgiya, Moscow, 1978.
19. Y. Liu, S. Sergey, Q. Han, L. Hua, and C. Xu: *Mater. Lett.*, 2012, vol. 67, pp. 52–55.
20. R. Folk, G. Fox, C.A. Shook, and C.W. Curtis: *J. Acoust. Soc. Am.*, 1958, vol. 30, pp. 552–58.
21. S.A.A. Mousavi, H. Feizi, and R. Madoliat: *J. Mater. Process. Technol.*, 2007, vols. 187–188, pp. 657–67.
22. Y. Liu, Q. Han, and L. Hua: in *Light Metals 2012*, C.E. Suarez, ed., TMS, Orlando, 2012, p. 259.
23. M.L. Wilkins and M.W. Guinan: *J. Appl. Phys.*, 1973, vol. 44, pp. 1200–06.
24. M.A. Meyers: *Dynamic Behavior of Materials*, Wiley-Interscience, New York, 1994, pp. 80–91.
25. R. Truel, C. Elbaum, and B. Chick: *Ultrasonics in Solid-State Physics*, Mir, Moscow, 1972.
26. R. Vepa: *Dynamics of Smart Structures*, Wiley, West Sussex, 2010, p. 546.
27. B. Langenecker, W.H. Frandsen, and A. Kennedy: *Tech. Prog. Rep.*, 1963, vol. 371, pp. 12–18.
28. I. Kristoffy: *J. Eng. Ind.*, 1969, vol. 1168, pp. 1174–86.
29. A.G. Rozner: *J. Acoust. Soc. Am.*, 1970, vol. 49, pp. 1368–78.
30. M.J. Adams, B.J. Briscoe, and S.K. Sinha: *Philos. Mag.*, 1996, vol. 74, pp. 1225–35.
31. G. Liu, J. Lu, and K. Lu: *Mater. Sci. Eng. A*, 2000, vol. 286, pp. 91–101.
32. Y.V.R.K. Prasad and K.P. Rao: *Mater. Sci. Eng. A*, 2004, vol. 374, pp. 335–45.
33. R.Z. Valiev, Y. Estrin, Z. Horita, T.G. Langdon, M.J. Zehetbauer, and Y.T. Zhu: *JOM*, 2006, vol. 4, pp. 33–40.
34. R.Z. Valiev and T.G. Langdon: *Prog. Mater. Sci.*, 2006, vol. 51, pp. 881–981.
35. B. Bay, N. Hansen, D.A. Hughes, and D. Kuhlmann-Wilsdorf: *Acta Metall. Mater.*, 1992, vol. 40, pp. 205–15.
36. V.F. Nesterenko, M.A. Meyers, and J.C. Lasalvia: *Mater. Sci. Eng. A*, 1997, vol. 229, pp. 23–36.
37. D.A. Hughes and N. Hansen: *Acta Mater.*, 1997, vol. 45, pp. 3871–82.
38. D.A. Hughes and N. Hansen: *Acta Mater.*, 2000, vol. 48, pp. 2985–97.
39. M.A. Meyers, V.F. Nesterenko, J.C. LaSalvia, and Q. Xue: *Mater. Sci. Eng. A*, 2001, vol. 317, pp. 204–18.
40. A. Mishra, B.K. Kad, F. Gregori, and M.A. Meyers: *Acta Mater.*, 2007, vol. 55, pp. 13–27.
41. Y. Iwahashi, Z. Horita, M. Nemoto, and T.G. Langdon: *Acta Mater.*, 1998, vol. 46, pp. 3317–28.
42. J.G. Sevillano, P.V. Houtte, and E. Aernoudt: *Prog. Mater. Sci.*, 1981, vol. 25, pp. 69–81.
43. D.A. Hughes, R.A. Lebensohn, H.R. Wenk, and A. Kumar: *Proc. R. Soc. Lond. A.*, 2000, vol. 456, pp. 921–28.
44. D. Kuhlmann-Wilsdorf and N. Hansen: *Scripta Metall. Mater.*, 1991, vol. 25, pp. 1557–63.
45. Q. Liu and N. Hansen: *Scripta Metall. Mater.*, 1995, vol. 32, pp. 1289–95.
46. D.A. Hughes, D.C. Chrzan, Q. Liu, and N. Hansen: *Phys. Rev. Lett.*, 1998, vol. 81, pp. 4664–70.
47. R.B. Lindsay: *Mechanical Radiation*, McGraw-Hill, New York, 1960, p. 586.
48. K.H. Westmacott and B. Langenecker: *J. Phys. Rev. Lett.*, 1965, vol. 14, pp. 221–22.
49. B.B. Rath and H. Hu: in *Nature and Behavior of Grain Boundaries*, H. Hu, ed., TMS Publication, Detroit, 1972, p. 405.
50. J.S. Koehler: *Imperfections in Nearly Perfect Crystals*, CRC Press, New York, 1952, p. 231.
51. A. Granato and K. Lucke: *J. Appl. Phys.*, 1956, vol. 27, pp. 583–94.
52. B.Y. Pines and I.F. Omel: *Dynamics of Dislocations, Proceedings of Finite*, SSR, Khar'kov, 1968.
53. B. Langenecker: *Rev. Sci. Instr.*, 1966, vol. 37, pp. 103–10.